

# MEMS Technology for Timing and Frequency Control

Clark T.-C. Nguyen

Dept. of Electrical Engineering and Computer Science  
University of Michigan

Ann Arbor, Michigan 48105-2122 USA

(presently on leave at DARPA, 3701 North Fairfax Drive, Arlington, VA 22203)

E-mail: [ctnguyen@umich.edu](mailto:ctnguyen@umich.edu)

**Abstract**—An overview on the use of microelectromechanical systems (MEMS) technologies for timing and frequency control is presented. In particular, micromechanical RF filters and reference oscillators based on recently demonstrated vibrating on-chip micromechanical resonators with  $Q$ 's >10,000 at 1.5 GHz, are described as an attractive solution to the increasing count of RF components (e.g., filters) expected to be needed by future multi-band wireless devices. With  $Q$ 's this high on-chip abundance, such devices might also enable a paradigm-shift in the design of timing and frequency control functions, where the advantages of high- $Q$  are emphasized, rather than suppressed (e.g., due to size and cost reasons), resulting in enhanced robustness and power savings. With even more aggressive three-dimensional MEMS technologies, even higher on-chip  $Q$ 's have been achieved via chip-scale atomic physics packages, which so far have achieved  $Q$ 's >10<sup>7</sup> using atomic cells measuring only 10 mm<sup>3</sup> in volume, consuming just 5 mW of power, all while still allowing Allan deviations down to 10<sup>-11</sup> at one hour.

**Keywords**—MEMS, micromechanical, quality factor, resonator, oscillator, filter, wireless communications, mechanical circuit, chip-scale atomic clock, physics package.

## I. INTRODUCTION

The performance of our electronic systems is generally limited by the accuracy and stability of the clocks or frequency references they use. For example, the ability and speed with which a GPS receiver can lock to a GPS satellite's pseudorandom signal and obtain position is dependent heavily upon how well synchronized its internal clock is to that of the satellite; here, the better the internal clock, the higher the probability and faster the lock. Unfortunately, our best clocks and frequency references (e.g., atomic clocks, oven stabilized crystal oscillators) are often too large or consume too much power to be used in portable applications. This forces us to keep our best electronic systems on tabletops and out of the hands of users, who must then access them through sometimes unreliable remote channels. Indeed, a technology capable of miniaturizing and lowering the power consumption of our best timekeepers and frequency references to the point of allowing insertion into truly portable applications would be most welcome.

In this regard, Micro Electro Mechanical Systems (MEMS) technology, with its ability to shrink mechanical

features and mechanisms down to micron (and even nano) scales, already provides substantial size and power reduction for applications spanning wireless communications [1][2], sensors, and fluidic systems, and is now emerging to provide similar advantages for frequency and timing references. In particular, vibrating micromechanical resonator devices based on silicon micromachining technologies have now been demonstrated with on-chip  $Q$ 's greater than 10,000 at GHz frequencies [3][4], frequency- $Q$  products exceeding 2.75×10<sup>13</sup> [3], temperature stability better than 18 ppm over 25 to 125°C [5], and aging stabilities better than 2 ppm over 1 year [6][7]. They have also been embedded into oscillator circuits to achieve phase noise performance satisfying GSM specifications for reference oscillators [8][9]. In addition, a combination of MEMS and micro-photonic technologies have now achieved 10 cm<sup>3</sup> complete atomic clocks consuming less than 200mW of power, while still attaining Allan deviations better than 5×10<sup>-11</sup> at 100s. Continued scaling of such devices that take advantage of compressed control time constants and lower heating power consumption is expected to soon yield complete atomic clocks in less than 1 cm<sup>3</sup>, consuming less than 30 mW of power, while still achieving Allan deviationd of 10<sup>-11</sup> at 1 hour.

This paper will describe not only how MEMS technologies have achieved the above, but also what other capabilities their integration density might enable for timing and frequency control in the coming years. After a brief introduction to MEMS fabrication technology, this paper expands upon this potential, then moves to describe some of the devices that might make it all possible.

## II. MEMS TECHNOLOGY

There are now a wide array of MEMS technologies capable of attaining on-chip micro-scale mechanical structures, each distinguishable by not only the type of starting or structural material used (e.g., silicon, silicon carbide, glass, plastic, etc.), but also by the method of micromachining (e.g., surface, bulk, 3D growth, etc.), and by the application space (e.g., optical MEMS, bio MEMS, etc.). For the present focus on timing and portable communications, MEMS technologies amenable to low capacitance merging of micromechanical structures together with integrated transistor circuits are of high interest.

---

Much of the described work was supported by DARPA and NSF.

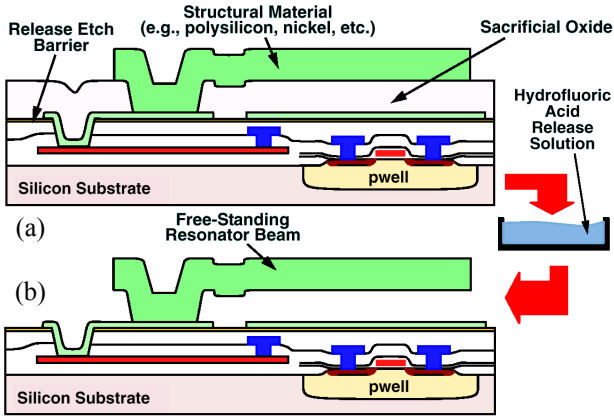


Fig. 1: Cross-sections (a) immediately before and (b) after release of a surface-micromachining process done directly over CMOS [10].

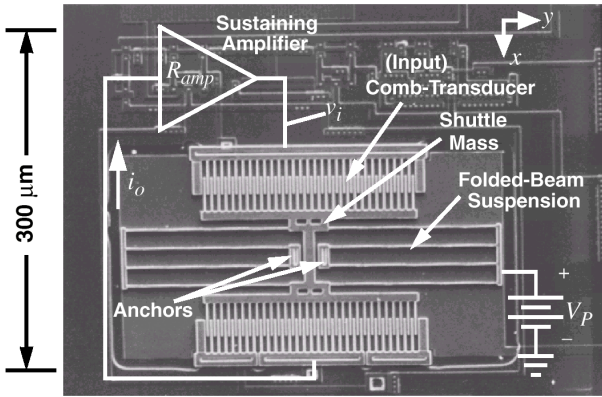


Fig. 2: SEM of a fully integrated 16-kHz watch oscillator that combines CMOS and MEMS in a single fully planar process [10].

With this in mind, Fig. 1 presents key cross-sections describing a polysilicon surface micromachining process done directly over silicon CMOS circuits in a modular fashion, where process steps for the transistor and MEMS portions are kept separate, in distinct modules. (Modularity is highly desirable in such a process, since a modular process can more readily adapt to changes in a given module, e.g., to a new CMOS channel length.) As shown, this process entails depositing and patterning films above a finished CMOS circuit using the same equipments already found in CMOS foundries until a cross section as in Fig. 1(a) is achieved. Here, the structural polysilicon layer has been temporarily supported by a sacrificial oxide film during its own deposition and patterning. After achieving the cross-section of Fig. 1(a), the whole wafer is dipped into an isotropic etchant, in this case hydrofluoric acid, which attacks only the oxide sacrificial layer, removing it and leaving the structural polysilicon layer intact, free to move.

Fig. 2 presents the SEM of a watch oscillator that combines a 16 kHz folded-beam micromechanical resonator with a  $Q$  of 50,000 together with sustaining CMOS transistor circuits using the very process flow of Fig. 1, but with tungsten as the metal interconnect in order to accommodate 625°C structural polysilicon deposition temperatures [10].

Although the use of tungsten instead of the more conventional copper and aluminum prevents the process of [10] from widespread use, other variants of this modular process have now been demonstrated that allow more conventional CMOS metals [11]. In addition, other non-modular merging processes [12] have already been used in integrated MEMS products for many years now. Whichever process is used, the size and integration benefits are clear, as the complete timekeeper of Fig. 2 measures only  $300 \times 300 \mu\text{m}^2$ , and could even be smaller if the transistors were placed underneath the micromechanical structure.

### III. INTEGRATED MICROMECHANICAL CIRCUITS

The MEMS-enabled integration density illustrated in Fig. 2 has the potential to shift paradigms that presently constrain the number of high- $Q$  components permissible in the design of present-day timing or frequency control functions, and instead allow the use of hundreds, perhaps thousands (or more), of high- $Q$  elements with negligible size or cost penalty. In particular, MEMS technology sports the attributes and ingredients to realize a micromechanical circuit technology that could reach large-scale integrated (LSI), or even very large-scale integrated (VLSI), proportions, the same way integrated circuit (IC) transistors had done over recent decades, and with potential for advances in capabilities in the mechanical domain as enormous as those achieved via the IC revolution in the electrical domain.

Note, however, that the ingredients required for a micromechanical circuit technology comprise much more than just small size. For example, the piezoelectric thin-film bulk acoustic resonators (FBAR's) [13][14] that have already become a successful high volume product in the wireless handset arena, although small, are perhaps not suitable for circuit design, since their frequencies are governed almost entirely by thickness, which is not a parameter that can be specified via computer-aided design (CAD) layout. Given how instrumental CAD has been to the success of VLSI transistor IC design, one would expect CAD-amenability to be equally important for micromechanical IC's. In this respect, the resonators and other elements in the repertoire of a micromechanical circuit design environment should have frequencies or other characteristics definable by *lateral* dimensions easily specifiable by CAD.

Continuing on this theme, a more complete set of attributes needed to effect a micromechanical circuit design environment can be listed as follows:

- 1) *CAD-amenable design.* For example, frequencies should be determined by lateral dimensions, which can be specified via CAD, not just vertical dimensions, which cannot. This makes possible an ability to attain many different frequencies in a single layer on a single-chip.
- 2) *Geometric flexibility.* Here, a given (often high) frequency should be attainable in a wide variety of shapes (e.g., beams, disks, etc.) and modes.
- 3)  $Q$ 's  $>1,000$  from 1–5000 MHz, with  $Q$ 's  $>10,000$  much

*preferred, if possible.*  $Q$ 's this high are needed to allow cascading of circuit blocks without accumulating excessive loss, and to allow channel-selection at RF.

- 4) *Thermal and aging stability to better than 2 ppm*, or at least amenable to compensation or control to this level.
- 5) *On/off switchability*. Here, the overriding preference is for vibrating micromechanical devices that can switch themselves, i.e., that do not require extra series switches, and that thus avoid the extra insertion loss.
- 6) *Massive-scale interconnectivity*. In some cases, several levels of both mechanical and electrical interconnect are desired.
- 7) *Nonlinear characteristics* that enable such functions as mixing, amplification, limiting, and other useful signal processing abilities.
- 8) *Amenability to low-capacitance single-chip integration with transistors*. This not only eliminates the impedance issue described previously, since the tiny magnitudes of on-chip parasitic capacitors allow impedances in the  $k\Omega$  range, but also affords designers a much wider palette of mechanical and electrical circuit elements.

As detailed in [1][2], a mechanical circuit technology with the attributes above might make possible filter banks capable of selecting channels (as opposed to just bands) right at RF with zero switching loss; oscillators using multiple high- $Q$  resonators to attain improved long- and short-term stability; oscillators with oven-control-like temperature stability, but consuming only milliwatts of power; ultra-low power completely mechanical RF front-ends for wireless handsets; and all of these realized on a single silicon chip.

Before expanding on some of the above, the next section first summarizes the basic resonator building blocks that might be used to implement such mechanical circuits.

#### IV. VIBRATING MICROMECHANICAL RESONATORS

Among the attributes listed above, the first two requiring CAD-amenability and geometric flexibility, are perhaps the most basic and the most difficult to achieve if constrained to macroscopic machining technologies. In particular, if GHz frequencies were required for flexural mode beams (for which the frequency is governed in part by length—a *lateral* dimension), then a macroscopic machining technology would be hard pressed to achieve such high frequencies. Fortunately, a major impetus behind MEMS technology stems from the fact that mechanical mechanisms benefit from the same scaling-based advantages that have driven the integrated circuit (IC) revolution in recent decades. Specifically, small size leads to faster speed, lower power consumption, higher complexity, and lower cost. And it does so not only in the electrical domain, but in virtually all other

**Table 1: High Frequency- $Q$  Product Vibrating RF MEMS Devices**

	Photo	Performance
CC-Beam Resonator [15]		Demo'ed: $Q \sim 8,000$ @ 10 MHz (vac) $Q \sim 50$ @ 10 MHz (air) $Q \sim 300$ @ 70 MHz (anchor diss.) $Q$ drop w/ freq. limits freq. range Series Resistance, $R_x \sim 5-5,000\Omega$
FF-Beam Resonator [16]		Demo: $Q \sim 28,000$ @ 10-200 MHz (vac) $Q \sim 2,000$ @ 90 MHz (air) No drop in $Q$ with freq. Freq. Range: >1GHz; unlimited w/ scaling and use of higher modes Series Resistance, $R_x \sim 5-5,000\Omega$
Wine-Glass Disk Res. [17]		Demo'ed: $Q \sim 156,000$ @ 60 MHz (vac) $Q \sim 8,000$ @ 98 MHz (air) Perimeter support design nulls anchor loss to allow extremely high $Q$ Freq. Range: >1GHz w/ scaling Series Resistance, $R_x \sim 5-5,000\Omega$
Contour-Mode Disk Res. [3][18]		Demo'ed: $Q \sim 11,555$ @ 1.5 GHz (vac) $Q \sim 10,100$ @ 1.5 GHz (air) Balanced design and material mismatching anchor-disk design nulls anchor loss Freq. Range: >1GHz; unlimited w/ scaling and use of higher modes Series Resistance, $R_x \sim 50-50,000\Omega$
Hollow Disk Ring Res. [4]		Demo'ed: $Q \sim 15,248$ @ 1.46 GHz (vac) $Q \sim 10,165$ @ 1.464 GHz (air) $\lambda/4$ notched support nulls anchor loss Freq. Range: >1GHz; unlimited w/ scaling and use of higher modes Series Resistance, $R_x \sim 50-5,000\Omega$

domains, including and especially mechanical. Although many examples of this from all physical domains exist, vibrating RF MEMS resonators perhaps provide the most direct example of how small size leads to faster speed in the mechanical domain.

#### A. High Frequency and $Q$

For example, on the macro-scale, a guitar string made of nickel and steel, spanning about 25" in length, and tuned to a musical "A" note, will vibrate at a resonance frequency of 110 Hz when plucked. In vibrating only at 110 Hz, and no other frequency, this guitar string is actually mechanically selecting this frequency, and is doing so with a  $Q$  on the order of 350, which is  $\sim 50X$  more frequency selective than a typical on-chip electrical *LC* tank. Of course, selecting a frequency like this is exactly what the RF and IF filters of a wireless phone must do, except they must do so at much higher frequencies, from tens of MHz to well into the GHz range. To achieve such frequencies with even better mechanical selectivity, dimensional scaling is needed. In particular, by shrinking a guitar string from 25" down to only 10μm, constructing it in stiffer, IC-compatible materials (like polysilicon), supporting it at nodes rather than at its ends (to minimize anchor losses), and exciting it electro-

statically or piezoelectrically rather than plucking it, one can achieve a free-free beam (“FF-beam”) resonator such as summarized in row 2 of Table 1 that resonates at frequencies around 100 MHz with  $Q$ ’s in excess of 10,000 [16][19].

In keeping with the scaling-based arguments presented so far, further scaling down to nano-dimensions does indeed yield frequencies in excess of 1 GHz [20]. However, as with nanoelectronics in the electrical domain, there are issues in the mechanical domain that might hinder the use of nanomechanical vibrating resonators (at least in their present form) for today’s communication purposes. In particular, excessive scaling may lead to “scaling-induced limitations”, such as adsorption-desorption noise [21], temperature fluctuation noise, and insufficient power handling. The first two of these can be mitigated by packaging the device under the right pressure and temperature conditions, but the last of these is perhaps more serious. As with nanoelectronics, the power handling issue with nanomechanical resonators really boils down to an impedance matching problem. In brief, nanostructures would rather operate at higher impedance levels than macroscopic counterparts, and in order to interface the nano with the macro (e.g., the antenna), impedance matching strategies like massive arraying of nanostructures to add their responses might be required.

Fortunately, nano-scale flexural mode beams need not be used to interface with macroscopic loads, as they are perhaps most useful as couplers between other elements in a micromechanical circuit. To interface with the macro-world, other geometries that allow GHz frequencies without the need for nano-scale dimensions can be used, such as the 1.51-GHz radial-contour mode disk in row 4 of Table 1, which achieves a record (at this frequency) room temperature  $Q$  of 11,555 in vacuum, and 10,100 in air. As shown more clearly in the schematic of Fig. 3, this resonator consists of a polydiamond disk suspended by a polysilicon stem at its very center, and completely surrounded by electrodes spaced less than 100 nm from its outer perimeter capable of electrostatically driving the disk into a mode shape where it expands and contracts along its radius, in a motion reminiscent of breathing [3][18][22]. The astonishingly high  $Q$  at greater than GHz frequencies is a result of the sheer symmetry of this disk design, and of a strategic impedance-mismatch between the polydiamond disk and polysilicon stem, both of which greatly suppress energy loss through the disk anchor [3]. Since the resonance frequency of this device goes approximately as the inverse of its radius, even higher frequency ( $>10$  GHz) with similar  $Q$ ’s is expected through radial scaling and the use of higher radial modes.

As detailed in [3], the use of diamond as the structural material for the radial mode resonator of row 4 in Table 1 contributes to the ease with which it achieves high frequency, since diamond’s acoustic velocity is twice that of silicon. However, diamond is not necessary to achieve  $Q$ ’s greater than 10,000 at frequencies past 1 GHz. Rather, as long as a properly impedance-mismatched resonator-to-anchor transition can be attained, polysilicon also works

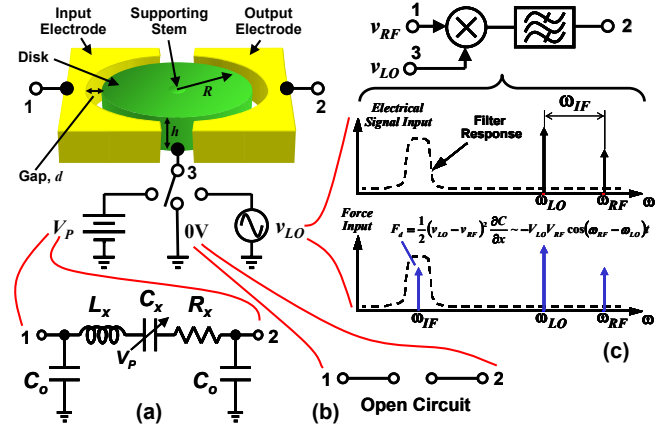


Fig. 3: Perspective-view schematic of the disk resonator of row 4 in Table 1, emphasizing the degree to which it is reconfigurable via the voltage applied to its bias port 3. Here, with  $V_3 = V_p$  the device is a high- $Q$  LCR; with  $V_3 = 0V$  the device is an open (i.e., is “off”); and with  $V_3 =$  a local oscillator signal  $v_{LO}$  the device becomes a mixer [25].

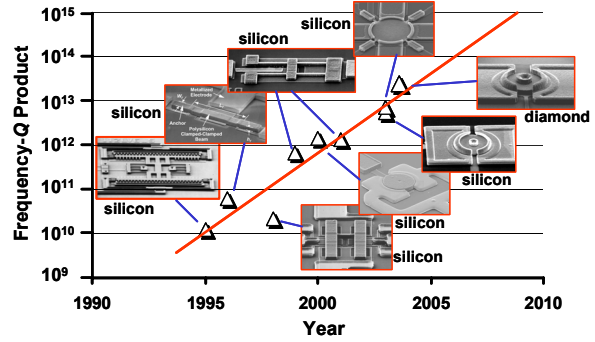


Fig. 4: Plot showing exponential growth in the frequency- $Q$  product of micromechanical resonators over time.

well, as demonstrated by a recent “hollow disk” extensional-mode ring resonator, shown in row 5 of Table 1. This device uses a centrally located support structure, attached to the ring at notched nodal locations and designed with dimensions corresponding to a quarter-wavelength of the ring resonance frequency, in order to reflect vibrational energy away from the central anchor and back into the ring. The ring itself vibrates extensionally by expanding and contracting along its inner and outer perimeter edges in a mode shape that allows very high frequency. With this design strategy, this polysilicon ring resonator achieves a  $Q$  of 14,603 at 1.2 GHz, which is the highest  $Q$  to date past 1 GHz for any on-chip resonator at room temperature [4][23][24]. The device is amenable to much higher frequency, as well, with a resonance frequency determined primarily by the width of the ring.

Fig. 4 presents a graph showing how the frequency- $Q$  product, a common figure of merit for resonators, has increased exponentially over recent years. At present, micro-mechanical disk resonators in CVD diamond structural material hold the record for frequency- $Q$  product, with a value of  $2.74 \times 10^{13}$  [3]. At the current rate of progress, the prospects for on-chip resonators operating past 10 GHz with  $Q$ ’s

>10,000 are not unreasonable in the next three years.

### B. Capacitive Transduction

Note that Table 1 contains all capacitively transduced devices, which in general offer the best frequency- $Q$  products among micromechanical resonator types, since they generally are constructed in single high quality materials, and thus suffer less from the material interface losses that can encumber other transducer types (e.g., piezoelectric). In addition to better  $Q$ , capacitive transduction also offers more flexible geometries with CAD-definable frequencies, voltage-controlled reconfigurability [25][26], better thermal stability [5], material compatibility with integrated transistor circuits, and an on/off self-switching capability [26], all of which contribute to the list of mechanical circuit-amenable attributes of the previous section.

The inherent on/off switchability (or “self-switching”) of a capacitively transduced device follows directly from the physics governing the output current sourced by such a device. In particular, to operate the disk of Fig. 3, the mechanical structure must be charged, in this case via the dc-bias voltage  $V_P$  (from which no dc current flows once the conductive structure is charged, so there is no dc power consumption). The voltage  $V_P$  generated by the charge effectively amplifies both the force imposed by the ac excitation signal  $v_i$  (applied to port 1) and the output motional current  $i_o$  generated (at port 2) by the dc-biased time-varying electrode-to-resonator capacitor that results when the disk vibrates. The transfer function from input to short-circuited output can be expressed as

$$\frac{i_o}{v_i}(s) = \frac{1}{R_x} \frac{(\omega_o/Q)s}{s^2 + (\omega_o/Q)s + \omega_o^2} \quad (1)$$

where  $\omega_o$  is its radian resonance frequency, and  $R_x$  is the series motional resistance of the device, given by

$$R_x = \frac{\sqrt{m_r k_r}}{Q} \frac{1}{V_P^2} \left[ \frac{\epsilon A_o}{d_o^2} \right]^2 = \frac{\sqrt{m_r k_r}}{Q} \frac{1}{V_P^2} \left[ \frac{2\pi\epsilon h R}{d_o^2} \right]^2 \quad (2)$$

where  $m_r$  and  $k_r$  are the equivalent mass and stiffness on the perimeter of the disk, respectively;  $\epsilon$  is the permittivity in the electrode-to-resonator gap;  $R$  and  $h$  are the disk radius and thickness, respectively, defined in Fig. 3;  $d_o$  is the electrode-to-resonator gap spacing; and  $A_o$  is the electrode-to-resonator overlap area. Recognizing (1) as the transfer function for a classic bandpass biquad, when “on” the micromechanical resonator of Fig. 3, and virtually all two-port vibrating mechanical resonators, can be modeled by the equivalent  $LCR$  electrical circuit shown in the figure.

From (2), when the dc-bias  $V_P$  is set to 0V, the series motional resistance  $R_x$  goes to infinity, making this device an effective open circuit. Thus, while other resonators require a (lossy) switch in series to be switched in or out of an electrical path, a capacitively-transduced micromechanical

**Table 2. Thermal Stability and Impedance of Microresonators**

	Photo		Performance
Electrical Stiff Comp. Res. [5]			Demo'ed: $Q \sim 4,000$ @ 10MHz (vac) Temperature-tailored gap to effect an electrical stiffness variation that cancels Young's modulus variation 18 ppm freq. variation over 27-107°C
SOI Silicon WG-Disk [27]		18μm-Thick SOI Disk	WGDisk: $Q \sim 26,000$ @ 149MHz (air) SiBAR: $Q \sim 40,000$ @ 137 MHz (vac) $Q \sim 3,700$ @ 983 MHz SOI thickness to effect large capacitive overlap for low Series Resistance, $R_x \sim 5.5k\Omega$ @ 137 MHz
Lateral Piezoelec Ring [28]		20 μm	Demo'ed: $Q \sim 2,900$ @ 473 MHz (air) Contour-mode ring-shaped AlN piezoelectric resonator Driven laterally via the $d_{31}$ coeff., so freqs. determined by lateral dims. Series Resistance, $R_x \sim 80\Omega$
Solid-Gap Disk Resonator [30]		Wine-Glass Disk With Solid Nitride-Filled Gap Disk Electrode 20-nm Nitride Gap	Demo'ed: $Q \sim 25,300$ @ 61MHz (vac) Solid nitride-filled electrode-to-resonator gap (20 nm) Much better yield and able to achieve low impedance at low dc-bias voltage Series Resistance, $R_x \sim 1.5k\Omega$ @ 4V

resonator can be switched in or out by mere application or removal the dc-bias  $V_P$  applied to its resonant structure. Note that this can now be done via a simple transistor switch (e.g., a pass gate), since this switching function is out of the signal path, making switch loss a non-issue.

### C. Thermal Stability, Aging, and Impedance

Besides frequency range and  $Q$ , thermal stability, aging/drift stability, and impedance, are also of utmost importance. Table 2 presents some of the micromechanical resonator devices designed specifically to address these parameters. In particular, the fixed-fixed beam device of row 1 in Table 2 utilizes a temperature-tailored top electrode-to-resonator gap spacing to attain a total frequency deviation over 25-125°C of only 18 ppm, which actually betters that of AT quartz. This, combined with recent demonstrations of good aging and drift [6][7], makes micromechanical resonators excellent candidates for reference oscillator applications in communication circuits. In addition, the devices of rows 2 and 3 illustrate strategies for lowering the impedances of stand-alone resonators, the first based on enlargement of the electrode-to-resonator capacitive overlap area to increase electromechanical coupling [27] (i.e., increasing  $A_o$  in (2)); the second dispensing with capacitive transducers, and using piezoelectric transducers [28][29]; with the latter being the more successful in achieving the 50-377Ω impedances desired for matching to off-chip wireless components.

Although it does achieve low impedance, and is amenable to CAD specification, the piezoelectric device of row 3 in Table 2 still sacrifices the important high  $Q$ , on/off self-

switching, and temperature stability attributes offered by capacitive transducers. To attain impedances similar to that of the row 3 device, yet retain capacitive transduction and all of its benefits, the device of row 4 has very recently been introduced. This 61-MHz wine-glass mode device is identical in shape and operation to that of row 3 in Table 1, but is now equipped with a solid dielectric-filled capacitive transducer gap (to replace the previous air gap) that reduces its impedance by  $8\times$  over its air-gap counterpart, while allowing it to retain a very high  $Q$  of 25,300 [30]. In addition to lower motional resistance, the use of solid dielectric-filled transducer gaps is expected to provide numerous other practical advantages over the air gap variety, since it (1) better stabilizes the resonator structure against shock and microphonics; (2) eliminates the possibility of particles getting into an electrode-to-resonator air gap, which poses a potential reliability issue; (3) greatly improves fabrication yield, by eliminating the difficult sacrificial release step needed for air gap devices; and (4) potentially allows larger micromechanical circuits (e.g., bandpass filters comprised of interlinked resonators) by stabilizing constituent resonators as the circuits they comprise grow in complexity.

## V. PURE MICROMECHANICAL CIRCUITS

Given that they satisfy all of the attributes listed in Section III, it is no surprise that capacitively transduced resonators have been used to realize the most complex micromechanical circuits to date. Table 3 summarizes several purely micromechanical circuits, from bandpass filters with impressive on-chip insertion losses of only 0.6dB for 0.09% bandwidth, some using non-adjacent bridging to effect loss poles [32]; to mixer-filter (“mixler”) devices that both translate and filter frequencies via a single passive structure [25]; to impedance transforming mechanically-coupled arrays that combine the responses of multiple high-impedance resonators to allow matching to a much lower  $50\Omega$  [33]; to a filter using mechanically-coupled composite resonators to allow matching to  $50\Omega$  while attaining the lowest insertion loss to date for a VHF micromechanical filter [34].

Each of the filters in Table 3 are comprised of several identical resonator elements coupled by mechanical links attached at very specific locations on the resonators. As detailed more fully in [15] and [31], the center frequency of such a mechanical filter is determined primarily by the

**Table 3: Summary of Vibrating Micromechanical Circuits**

	Photo	Data	Performance
3-Res. Folded-Beam Filter [31]	<p>Folded-Beam μMech. Resonator Mass Control Holes Coupling Beam</p>	<p>Transmission [dB] Frequency [kHz]</p>	Freq. = 340 kHz BW = 403 Hz %BW = 0.09% StopB Rej. = 64 dB Ins. Loss < 0.6 dB
Mixer-Filter [25]	<p>Local Oscillator Port Nonconductive Coupling Beam RF Port IF Port Input Resonator Output Resonator</p>	<p>Uncalibrated Amplitude [dB] Frequency [MHz]</p>	Mixes a 240MHz RF down to 37MHz IF, then filters Conv. Loss = 9.5dB %BW = 1.7% Ins. Loss = 3.5dB
3 Res. Bridged CC-Beam [32]	<p>Bridging Coupler In Out</p>	<p>Transmission [dB] Frequency [MHz]</p>	Freq. = 9 MHz BW = 20 kHz %BW = 0.2% StopB Rej. = 51 dB Ins. Loss < 2.8 dB
Mech.-Coupled Res. Array [33]	<p>Mechanical Coupling Point Square Plate Resonator</p>	<p>Current [μA] Frequency [MHz]</p>	Automatic matching of resonators achieved via mech. coupling; current multiplied by number of resonators $N$
Array Composite Filter [34]	<p>Mechanically Coupled Array Composite Resonator Square-Plate Micromechanical Resonator Coupling Beam</p>	<p>Transmission [dB] Frequency [MHz]</p>	Freq. = 68.1 MHz BW = 190 kHz %BW = 0.28% StopB Rej. = 25 dB Ins. Loss < 2.7 dB

(identical) frequencies of its constituent resonators, while the spacings between modes (i.e., the bandwidth) is determined largely by a ratio of the stiffnesses of its coupling beams to that of the resonators they couple at their attachment locations. The circuit nature of each filter in Table 3 is emphasized by the fact that each was designed using equivalent electrical circuits defined by electromechanical analogies [15][31], which allowed the use of electrical circuit simulators, like SPICE—an important point that implies mechanical circuits should be amenable to the vast automated circuit design environments already in existence.

The arraying used in the devices of rows 4 and 5 not only provides a lower filter termination impedance by increasing the effective capacitive transducer overlap area, but also raises the 3<sup>rd</sup> order intermodulation intercept point ( $I_{IP3}$ ) of the composite device [35][36] (i.e., raises its linearity) in the process. Fig. 5 further illustrates how arraying can achieve a much larger increase in capacitive transducer overlap area than a single device specially designed for larger transducer area—a clear example of how a circuit technique can be superior to the use of a single “advanced” device. The similarities between the described arraying approach and similar strategies in transistor integrated circuit design are noteworthy. In particular, the use of an array of

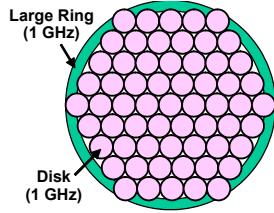


Fig. 5: Illustration showing that, in the same footprint, an array of small 1GHz disks can achieve a larger sidewall surface area (hence, larger electromechanical coupling and smaller filter impedance) than a single 1GHz ring made large to minimize impedance.

resonators to match the impedance of a micromechanical circuit to an off-chip macroscopic element (e.g., an antenna) is really no different from the use of a cascade of progressively larger inverters (or actually, in layout, arrays of smaller inverters) to allow a minimum-sized digital gate to drive an off-chip board capacitor. In essence, micro (or nano) scale circuits, whether they be electrical or mechanical, prefer to operate with higher impedances than macro-scale ones, and interfacing one with the other requires a proper impedance transformation. In a building block circuit environment, such an impedance transformation is most conveniently accomplished via large numbers of circuit elements, whether they be electronic transistors or mechanical resonators.

Table 3 also implicitly indicates the progression of micromechanical circuit complexity with time. In particular, the composite array filter in row 5 uses more than 43 resonators and links, which qualifies it as a medium-scale integrated (MSI) micromechanical circuit. And this is just the beginning. After all, the aforementioned RF channel-select filter banks [1][2] aim to use hundreds or thousands of filters like this, which would inevitably lead to LSI or VLSI micromechanical circuits. When combined (preferably on the same chip [10][11][12]) with transistor integrated circuits, the time domain prowess of transistors can be merged with the frequency domain capabilities of mechanical circuits to achieve even greater functionality.

## VI. MICROMECHANICAL RESONATOR OSCILLATORS

Leeson's equation [37] indicates that the stability of an oscillator, as measured by its phase noise, is inversely proportional to the  $Q$  of its frequency setting tank element. Given that the micromechanical disk and ring resonators of rows 4 and 5 of Table 1 have posted the highest room temperature  $Q$ 's of any on-chip resonator around 1 GHz to date, the use of MEMS technology in compact LO implementations is fully expected to yield substantial improvements in LO performance. In particular, according to Leeson's equation, if a present-day VCO attains -121 dBc/Hz at a 600 kHz offset from an 1.8 GHz carrier using an  $LC$  tank with a  $Q$  of 30, then the use of a vibrating micromechanical disk resonator with a  $Q$  of 10,000 should provide ~50 dB of improvement, or -171 dBc/Hz at a 600 kHz carrier offset (provided the thermal noise floor allows it, that is).

To date, work towards demonstrating the above GHz oscillator using a micromechanical resonator tank is ongoing. However, a lower frequency reference oscillator based on a 61-MHz wine-glass-mode disk resonator (row 3 of Table 1

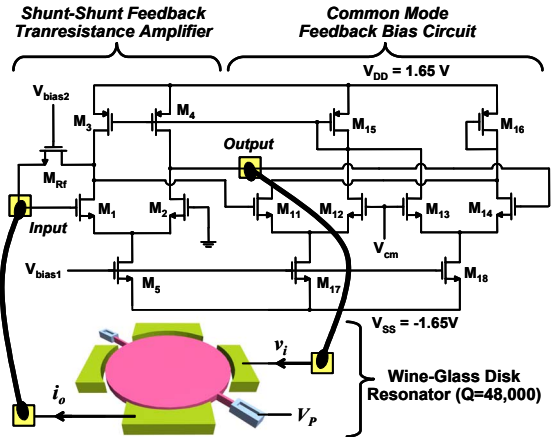


Fig. 6: Circuit schematic of a 61-MHz series resonant reference oscillator using a wine-glass disk resonator frequency-setting element with a  $Q$  of 48,000 in vacuum, and 10,000 in air [9].

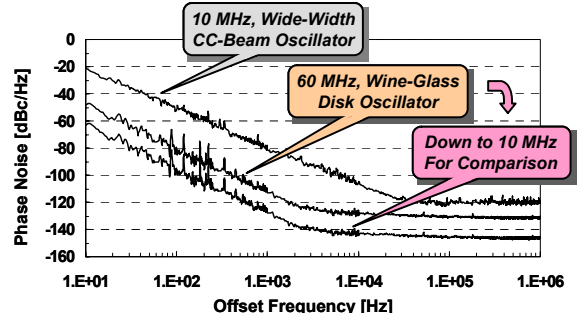


Fig. 7: Comparison of measured phase noise density versus carrier offset for the oscillator circuit of [9] paired with a 10-MHz CC-beam oscillator and a 61-MHz wine-glass disk oscillator, with an extrapolation for the latter down to 10 MHz for fair comparison.

[17]) was recently published that consumed  $350\mu\text{W}$  of power towards phase noise marks at 1kHz and far-from-carrier offsets of -110 and -132 dBc/Hz, respectively [9]. Fig. 6 presents the circuit schematic and Fig. 7 the measured phase noise plot for this oscillator. As indicated in the plot, when translated down to 10MHz for fair comparison, these values equate to -125 and -147, respectively [9], both of which satisfy or nearly satisfy (depending on who you talk to) the needs of GSM cellular phones. With a resonator  $Q$  of 48,000, this oscillator was actually expected to perform much better, even when operating with such low power consumption. Unfortunately, however, an unexpected  $1/f^2$  noise component introduced itself at close-to-carrier offsets, most likely caused by resonator nonlinearities involved in the oscillation amplitude limiting process. Other work [38] indicates that this  $1/f^2$  component can be removed (leaving the expected  $1/f^2$ ) by designing so that limiting occurs through transistor circuit nonlinearity, not resonator nonlinearity. It is expected that this will be easier to do at GHz frequencies, since higher frequency resonators are stiffer and can handle larger powers than the VHF wine-glass disk of Fig. 6.

In the meantime, a more elegant solution to improving the close-to-carrier phase noise of lower frequency oscillators

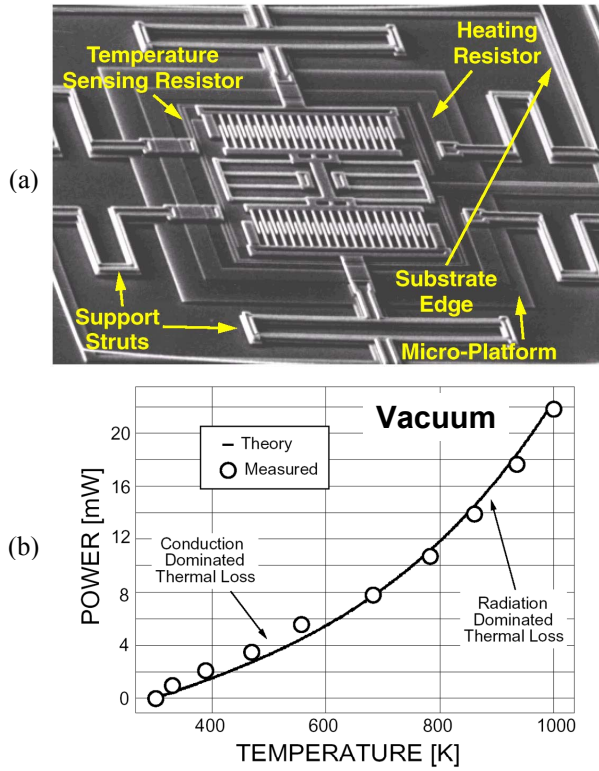


Fig. 8: (a) SEM of a fabricated folded-beam micromechanical resonator mounted on a micro-oven platform. (b) Measured power required to achieve a given temperature. Here, only 2 mW is required to achieve 130°C [41].

tors based on the mechanically-coupled array method of row 4 in Table 3 has now been demonstrated. In particular, the use of several resonators in a mechanically-coupled array that locks all resonator frequencies to one mode, hence permits summing of all their outputs, has provided up to 40dB of phase noise improvement for the oscillator of [39], and has very recently yielded a surface-micromachined disk-array oscillator that more than satisfies the GSM reference oscillator phase noise specifications [40]. These results illustrate yet again how the use of many high-*Q* elements in an interlinked mechanical circuit can propel performance.

#### A. Micro-Oven Control

In addition to good short-term stability, MEMS technology has great potential to achieve oscillators with excellent thermal stability. In particular, the tiny size and weight of vibrating micromechanical resonators allow them to be mounted on micro-platforms suspended by long thin tethers with thermal resistances many orders of magnitude larger than achievable on the macro-scale. Such a large thermal resistance to its surroundings then allows the platform and its mounted contents to be heated to elevated temperatures with very little power consumption (e.g., milliwatts). Fig. 8 presents the first such platform-mounted folded-beam micromechanical resonator, where the nitride platform supporting the resonator also included thermistor and heating resistors that when embedded in a feedback loop maintained the temperature of the platform at 130°C with only 2mW of

total power consumption [41]. With oven-controlling feedback engaged, the temperature coefficient of the platform-mounted micromechanical resonator was reduced by more than 5 times, with thermally induced warping of the platform the performance limiter. Much better reduction factors are expected with a more refined platform design.

## VII. CHIP-SCALE ATOMIC CLOCKS

Although the described micromechanical resonator oscillators are expected to achieve excellent phase noise performance at carrier offsets greater than 100 Hz, and micro-oven control might soon allow them to reach temperature stabilities down to  $10^{-9}$  (and maybe even better), their aging rates will likely not match those of atomic clocks. Unless atomic clocks with stability better than  $10^{-11}$  over one hour can be shrunk from the 9,000 cm<sup>3</sup>, 60 W commercial units existing today, down to a more portable size and battery drain, our best electronic systems (which rely on the accuracy and precision of atomic clocks) will remain on tabletops, and out of the hands of the individual user. With the intent of changing this, the Chip-Scale Atomic Clock (CSAC) program in the Microsystems Technology Office (MTO) of the Defense Advanced Research Projects Agency (DARPA) in the U.S. is attempting to harness MEMS and microphotonics technologies to miniaturize atomic clocks down to a more-than-portable 1 cc size, while still achieving  $10^{-11}$  Allan deviation over one hour with less than 30 mW of power. These goals represent a more than 9,000× reduction in volume, and 2,000× reduction in power consumption, versus the small atomic clocks in the market at the 2002 start of the CSAC program.

Like quartz or vibrating resonator oscillators and clocks, atomic clocks function by generating a very stable frequency off of a very stable reference. The main difference is that a quartz oscillator derives its frequency from a mechanically vibrating reference, which makes its frequency subject to long-term changes in mechanical dimensions and stress. An atomic clock, on the other hand, derives its frequency from the energy difference between the hyperfine states of an alkali metal atom, which is a constant of nature, and thereby, much more predictable and stable.

Among the existing approaches to realizing an atomic clock, the vapor cell method depicted schematically in Fig. 9 is perhaps the most amenable to miniaturization. Here, a cell containing the alkali metal in a sufficiently dense vapor state is interrogated by a laser at a wavelength absorbed by the vapor (i.e., that excites the single outer orbital electron to the next orbital; 894 nm for the cesium D1 line). A photodetector at the other end of the vapor cell monitors the intensity of the laser light. Energy at the frequency that excites the hyperfine transition, given by  $\Delta E = h\nu$ , where  $h$  and  $\nu$  are Planck's constant and the characteristic frequency, respectively; is then pumped into the system in one of two ways (either of which can work at the micro-scale): (1) electromagnetically, via an RF signal at frequency  $\nu$ ; or (2) optically, by modulating the laser at the needed frequency  $\nu$ .

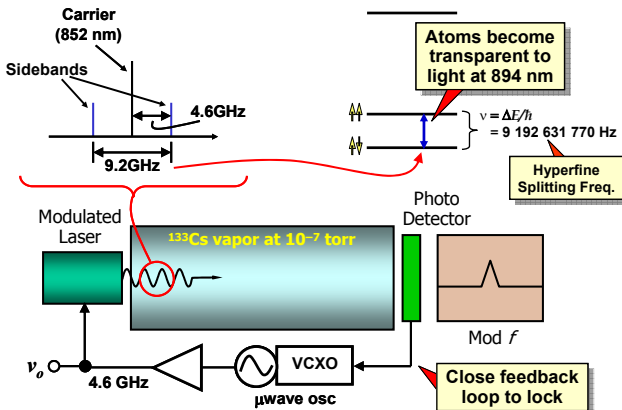


Fig. 9: Schematic describing the basic topology of a vapor cell-based atomic clock, this one exciting the hyperfine resonance via a laser-modulated approach dubbed coherent population trapping (CPT).

Fig. 9 uses the latter method, where modulation of the laser at the hyperfine splitting frequency ( $v=9.192631770$  GHz, for cesium) excites the atoms into a coherent state, where they become transparent to the interrogating laser light (i.e., they no longer absorb it), inducing a peak in the intensity of the laser light. A microwave oscillator capable of delivering the needed output power is then locked to the (very accurate) hyperfine splitting frequency via a feedback circuit that controls the oscillator frequency so that the photodetector intensity is maximized at the hyperfine peak.

#### A. Reducing Power Consumption Via Scaling

As mentioned, the alkali metal atoms must be maintained at a sufficient density in a vapor state to operate the atomic clock, which means power must be consumed to heat the vapor cell that contains the atoms. For a tabletop atomic clock, this can take tens of watts of power. Obviously, any approach to reducing the total clock power consumption down to 30 mW must include a strategy for reducing this heating power by three orders of magnitude.

Once again, as with the vibrating resonators of Section IV, smaller is better. In particular, for the case of a vapor cell-based atomic clock, scaling a Cs- or Rb-filled atomic cell to millimeter or even micron dimensions greatly reduces the power required to maintain the cell at the elevated temperature needed to keep the atoms in a sufficiently dense vapor state. The power savings can be enormous, as illustrated in Fig. 10, which compares the powers required to maintain (in vacuum) a temperature of 80°C on a small macro-cell, about 2 cm in diameter, an on a tiny micro-cell, measuring just 300 μm on a side, assuming that conduction is the dominant heat loss mechanism. Given that the micro-scale cell weighs so little, it can be supported by tethers so long and thin that they achieve thermal resistances  $R_{th}$  on the order of 61,000 K/W, to be compared with the 18 K/W that might be seen on the macro-scale. These differences in thermal isolation lead to a micro-cell power requirement for 80°C of only 1 mW, which is 3000× smaller than the 3W that would be required for the small macro-cell. Furthermore,

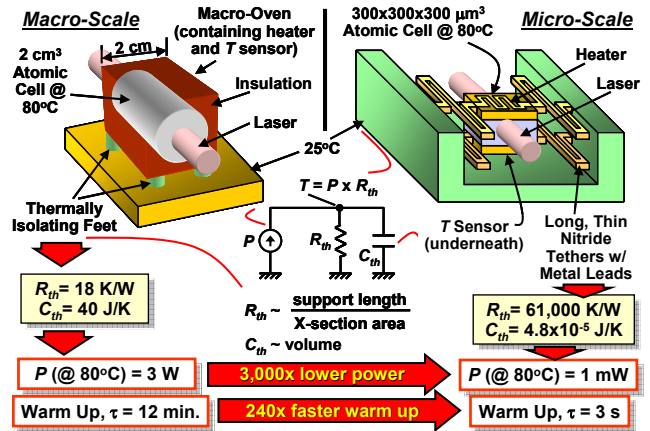


Fig. 10: Schematics summarizing the analytical determination of the powers required to maintain macro and micro vapor cells at 80°C in vacuum. Here, the equivalent thermal circuit used also yields warm up times.

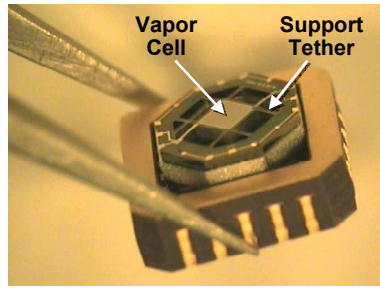


Fig. 11: Tiny physics package by Symmetricom/Draper/Sandia, featuring a tiny atomic vapor cell supported by long thin thermally isolating tethers that allow heating to 80°C with less than 5 mW of heating power.

more, due to the tiny volume of the micro-cell, and thus tiny thermal capacitance on the order of  $10^{-5}$  J/K, the warm up time for the micro-cell of only 3 seconds is 240× faster than the 12 minutes typical of macro-scale atomic clocks.

It should be noted that the above illustration considered only conductive heat loss for simplicity. In actuality, the conductive heat loss for the tether-supported micro-cell is so small that radiation heat loss becomes dominant at 80°C. This radiation heat loss, however, is also small, so that the actual micro-atomic tether-supported cell by the Symmetricom/Draper team in the CSAC program, shown in Fig. 11, still requires only 5 mW of power to maintain a temperature of 80°C in its vacuum enclosure [42].

#### B. Scaling Limits

But along with its benefits, scaling also introduces some potential disadvantages. In particular, among the more troublesome disruptors of stability in a gas-cell atomic clock are collisions between the atomic gas species and the walls, which can dephase the atoms, disrupting their coherent state. Because shrinking an atomic cell amounts to raising its surface-to-volume ratio, hence, making its walls look much larger to the atoms, one might expect an increase in atom-to-wall collisions to degrade the  $Q$  of an atomic cell as it is scaled to millimeter or micro-scale dimensions. Fortunately, however, the judicious use of the right buffer gases

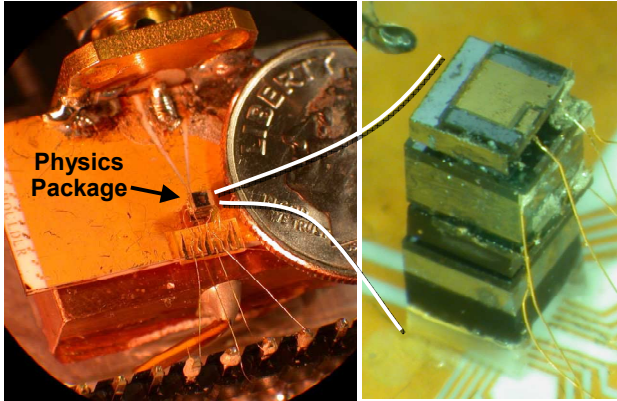


Fig. 12: Chip-scale atomic physics package by NIST, occupying less than  $10 \text{ mm}^3$  in volume.

to lower the mean free path of “clock” atoms so that they rarely reach the walls, but rather “soft impact” the buffer gases, allows a designer to shrink vapor cell dimensions down to 100’s of microns while maintaining a low enough atom-to-wall collision rate to allow clock performance down to  $10^{-11}$  Allan deviation at one hour.

Fig. 12 presents photos of one of the smallest physics packages ever built (by NIST [43]), occupying just  $10 \text{ mm}^3$  in volume, and comprising a tiny micromachined atomic vapor cell [43] containing either Cs or Rb, an interrogating VCSEL working preferably on the D1 line, a photodiode detector, polarizing and focusing optics, heater elements to maintain atoms in a sufficiently dense vapor state, and a micromechanical suspension system that thermally isolates the vapor cell/heater structure to allow elevated temperatures with low power consumption. The thermal isolation for this physics package is not quite as good as that of Fig. 11, so its power consumption is on the order of 75 mW, but its tiny vapor cell so far has permitted measured Allan deviations better than  $10^{-11}$  at one hour.

### C. Tiny Atomic Clocks

Fig. 13 presents the Allan deviation plot and photo of a completely self-contained atomic clock by the Symmetricon/Draper/Sandia team in the CSAC program that occupies only  $9.95 \text{ cm}^3$ , yet achieves an Allan deviation of  $5 \times 10^{-11}$  at 100s, while consuming less than 153 mW of power. This is the smallest, lowest power atomic clock in existence to date. But it won’t remain so long; in particular, if things go as planned in the CSAC program,  $1 \text{ cm}^3$  versions consuming only 30 mW while attaining  $10^{-11}$  at one hour Allan deviation will likely surface soon.

## VIII. CONCLUSIONS

MEMS-based realizations of timing and frequency control functions, including 0.09% bandwidth filters with less than 0.6dB insertion loss, GSM-compliant low phase noise oscillators, and miniature atomic clocks posting  $5 \times 10^{-11}$  at 100s Allan deviation (so far) and consuming only 153 mW, have been described with an emphasis on the performance

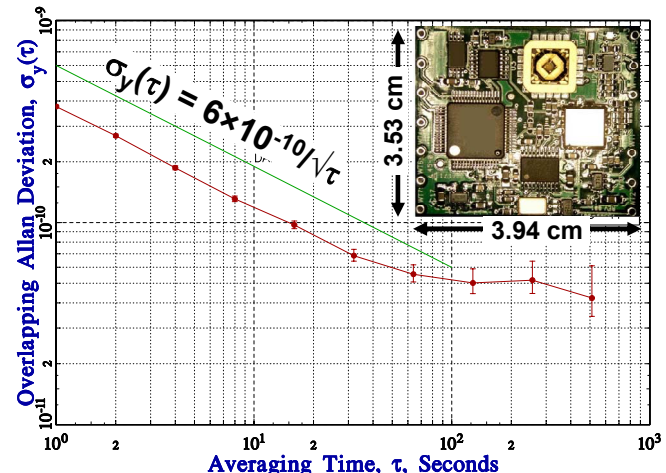


Fig. 13: Measured Allan deviation plot for the output of the  $9.95 \text{ cm}^3$  atomic clock by the Symmetricon/Draper/Sandia team.

benefits afforded by scaling to micro dimensions. In particular, via scaling, vibrating RF MEMS devices have now reached frequencies commensurate with critical RF functions in wireless applications and have done so with previously unavailable on-chip  $Q$ ’s exceeding 10,000.  $Q$ ’s this high may now encourage paradigm-shifting communication architectures that can eliminate interferers immediately after the antenna, allowing subsequent electronics to operate with much lower dynamic range and power consumption than would otherwise be needed. Given present transistor scaling trends towards lower dynamic range digital devices, such a relaxation in dynamic range requirements may be arriving at an opportune time.

In the meantime, the success of efforts to scale atomic clocks down to  $10 \text{ cm}^3$  (so far) strongly encourages ongoing efforts bent on shrinking them even further, down to  $1 \text{ cm}^3$  volume, while still posting  $10^{-11}$  Allan deviation at one hour with less than 30 mW of power consumption.

## REFERENCES

- [1] C. T.-C. Nguyen, “Transceiver front-end architectures using vibrating micromechanical signal processors,” chapter in *RF Technologies for Low Power Wireless Communications*, edited by G. I. Haddad, T. Itoh, and J. Harvey, pp. 411-461. New York: Wiley IEEE-Press, 2001.
- [2] C. T.-C. Nguyen, “Vibrating RF MEMS overview: applications to wireless communications (invited),” *Proceedings, Photonics West: MOEMS-MEMS 2005*, San Jose, California, Jan. 22-27, 2005, Paper No. 5715-201.
- [3] J. Wang, J. E. Butler, T. Feygelson, and C. T.-C. Nguyen, “1.51-GHz polydiamond micromechanical disk resonator with impedance-mismatched isolating support,” *Proceedings, IEEE Int. MEMS Conf.*, Maastricht, The Netherlands, Jan. 25-29, 2004, pp. 641-644.
- [4] S.-S. Li, Y.-W. Lin, Y. Xie, Z. Ren, and Clark T.-C. Nguyen, “Micromechanical hollow-disk ring resonators,” *Proceedings, 17th Int. IEEE MEMS Conf.*, Maastricht, Netherlands, Jan. 25-29, 2004, pp. 821-824.
- [5] W. -T. Hsu and C. T. -C. Nguyen, “Stiffness-compensated temperature-insensitive micromechanical resonators,” *Tech. Digest, 2002 IEEE Int. MEMS Conf.*, Las Vegas, Nevada, Jan. 20-24, 2002, pp. 731-734.
- [6] V. Kaajakari, J. Kiihamäki, A. Oja, H. Seppä, S. Pietikäinen, V. Kokkala, and H. Kuisma, “Stability of wafer level vacuum encapsulated single-crystal silicon resonators,” *Digest of Technical Papers, Int. Conf.*

- on Solid-State Sensors, Actuators, and Microsystems (Transducers'05), Seoul, Korea, June 2005, pp. 916-919.
- [7] B. Kim, R. N. Candler, M. Hopcroft, M. Agarwal, W.-T. Park, and T. W. Kenny, "Frequency stability of wafer-scale encapsulated MEMS resonators," *Digest of Technical Papers*, Int. Conf. on Solid-State Sensors, Actuators, and Microsystems (Transducers'05), Seoul, Korea, June 2005, pp. 1965-1968.
- [8] V. Kaajakari, T. Mattila, A. Oja, J. Kiihamäki, and H. Seppä, "Square-extensional mode single-crystal silicon micromechanical resonator for low-phase-noise oscillator applications," *IEEE Electron Device Letters*, vol. 25, no. 4, pp. 173-175, April 2004.
- [9] Y.-W. Lin, S. Lee, S.-S. Li, Y. Xie, Z. Ren, C. T.-C. Nguyen, "Series-resonant VHF micromechanical resonator reference oscillators," *IEEE J. Solid-State Circuits*, vol. 39, no. 12, pp. 2477-2491, Dec. 2004.
- [10] C. T.-C. Nguyen and R. T. Howe, "An integrated CMOS micromechanical resonator high-Q oscillator," *IEEE J. Solid-State Circuits*, vol. 34, no. 4, pp. 440-455, April 1999.
- [11] A. E. Franke, J. M. Heck, T.-J. King and R. T. Howe, "Polycrystalline silicon-germanium films for integrated microsystems," *IEEE/ASME J. Microelectromech. Syst.*, vol. 12, no. 2, pp. 160-171, April 2003.
- [12] T. A. Core, W. K. Tsang, and S. J. Sherman, "Fabrication technology for an integrated surface-micromachined sensor," *Solid State Technology*, pp. 39-47, Oct. 1993.
- [13] R. C. Ruby, P. Bradley, Y. Oshmyansky, A. Chien, and J. D. Larson III, "Thin film bulk wave acoustic resonators (FBAR) for wireless applications," *Proceedings*, IEEE Int. Ultrasonics Symposium, Atlanta, GA, 2001, pp. 813-821.
- [14] H. Yu, *et al.*, "Film bulk acoustic resonator at 4.4 GHz with ultra low temperature coefficient of resonant frequency," *Tech. Dig.*, 18<sup>th</sup> IEEE Int. Conf. on MEMS, Miami Beach, Florida, Jan. 30-Feb. 3, 2005, pp. 28-31.
- [15] F. D. Bannon III, J. R. Clark, and C. T.-C. Nguyen, "High frequency micromechanical filters," *IEEE J. Solid-State Circuits*, vol. 35, no. 4, pp. 512-526, April 2000.
- [16] K. Wang, A.-C. Wong, and C. T.-C. Nguyen, "VHF free-free beam high-Q micromechanical resonators," *IEEE/ASME J. Microelectromech. Syst.*, vol. 9, no. 3, pp. 347-360, Sept. 2000.
- [17] M. A. Abdelmoneum, M. U. Demirci, and C. T.-C. Nguyen, "Stemless wine-glass-mode disk micromechanical resonators," *Proceedings*, 16th Int. IEEE MEMS Conf., Kyoto, Japan, Jan. 19.-23, 2003, pp. 698-701.
- [18] J. Wang, Z. Ren, and C. T.-C. Nguyen, "1.156-GHz self-aligned vibrating micromechanical disk resonator," *IEEE Trans. Ultrason., Ferroelect., Freq. Contr.*, vol. 51, no. 12, pp. 1607-1628, Dec. 2004.
- [19] M. U. Demirci and C. T.-C. Nguyen, "Higher-mode free-free beam micromechanical resonators," *Proceedings*, 2003 IEEE Int. Frequency Control Symposium, Tampa, Florida, May 5-8, 2003, pp. 810-818.
- [20] X. M. H. Huang, C. A. Zorman, M. Mehregany, M. L. Roukes, "Nanodevice motion at microwave freqs," *Nature*, vol. 421, pg. 496, Jan. 30, 2003.
- [21] J. R. Vig and Y. Kim, "Noise in microelectromechanical system resonators," *IEEE Trans. Ultrason. Ferroelec. Freq. Contr.*, vol. 46, no. 6, pp. 1558-1565, Nov. 1999.
- [22] J. Wang, Z. Ren, and C. T.-C. Nguyen, "Self-aligned 1.14-GHz vibrating radial-mode disk resonators," *Dig. of Tech. Papers*, Transducers'03, Boston, Massachusetts, June 8-12, 2003, pp. 947-950.
- [23] B. Bircumshaw, G. Lui, H. Takeuchi, T.-J. King, R. T. Howe, O. O'Reilly, and A. P. Pisano, "The radial bulk annular res.: towards a 50Ω MEMS filter," *Dig. of Tech. Papers*, Transducers'03, Boston, Massachusetts, June 8-12, 2003, pp. 875-878.
- [24] Y. Xie, S.-S. Li, Y.-W. Lin, Z. Ren, and C. T.-C. Nguyen, "UHF Micromechanical Extensional Wine-Glass Mode Ring Resonators," *Technical Digest*, 2003 IEEE International Electron Devices Meeting, Washington, DC, Dec. 8-10, 2003, pp. 953-956.
- [25] A.-C. Wong and C. T.-C. Nguyen, "Micromechanical mixer-filters ("mixlers")," *IEEE/ASME J. Microelectromech. Syst.*, vol. 13, no. 1, pp. 100-112, Feb. 2004.
- [26] S.-S. Li, Y.-W. Lin, Z. Ren, and C. T.-C. Nguyen, "Self-switching vibrating micromechanical filter bank," *Proceedings*, IEEE Combined Int. Frequency Control/Precision Time & Time Interval Symposium., Vancouver, Canada, Aug. 29-31, 2005, to be published.
- [27] S. Pourkamali, *et al.*, "Vertical capacitive SiBARs," *Tech. Dig.*, 18<sup>th</sup> IEEE Int. Conf. on MEMS, Miami Beach, Florida, Jan. 30-Feb. 3, 2005, pp. 211-214.
- [28] G. Piazza, *et al.*, "Low motional resistance ring-shaped contour-mode aluminum nitride piezoelectric micromechanical resonators for UHF applications," *Tech. Dig.*, 18<sup>th</sup> IEEE Int. Conf. on MEMS, Miami Beach, Florida, Jan. 30-Feb. 3, 2005, pp. 20-23.
- [29] D. T. Chang, *et al.*, "A new MEMS-based quartz resonator technology," *Tech. Dig.*, Solid-State Sensor, Actuator, and Microsystems Workshop, Hilton Head, South Carolina, June 6-10, pp. 41-44.
- [30] Y.-W. Lin, S.-S. Li, Z. Ren, and C. T.-C. Nguyen, "Vibrating micromechanical resonators with solid dielectric capacitive-transducer 'gaps,'" *Proceedings*, IEEE Combined Int. Frequency Control/Precision Time & Time Interval Symposium., Vancouver, Canada, Aug. 29-31, 2005, to be published.
- [31] K. Wang and C. T.-C. Nguyen, "High-order medium frequency micromechanical electronic filters," *IEEE/ ASME J. Microelectromech. Syst.*, vol. 8, no. 4, pp. 534-557, Dec. 1999.
- [32] S.-S. Li, *et al.*, "Bridged micromechanical filters," *Proceedings*, IEEE Int. Ultrasonics, Ferroelectrics, and Freq. Control 50th Anniv. Joint Conf., Montreal, Canada, Aug. 24-27, 2004, pp. 144-150.
- [33] M. U. Demirci, *et al.*, "Mech. corner-coupled square microresonator array for reduced series motional resistance," *Dig. of Tech. Papers*, Transducers'03, Boston, MA, June 8-12, 2003, pp. 955-958.
- [34] M. U. Demirci and C. T.-C. Nguyen, "A low impedance VHF micromechanical filter using coupled-array composite resonators," *Dig. of Tech. Papers*, the 13th Int. Conf. on Solid-State Sensors & Actuators (Transducers'05), Seoul, Korea, June 5-9, 2005.
- [35] R. Navid, J. R. Clark, M. Demirci, and C. T.-C. Nguyen, "Third-order intermodulation distortion in capacitively-driven CC-beam micromechanical resonators," *Tech. Digest*, 14<sup>th</sup> Int. IEEE MEMS Conf., Interlaken, Switzerland, Jan. 21-25, 2001, pp. 228-231.
- [36] Y.-W. Lin, S.-S. Li, Z. Ren, and C. T.-C. Nguyen, "Third-order intermodulation distortion in capacitively-driven VHF micromechanical resonators," *Proceedings*, IEEE Ultrasonics Symposium, Sept. 18-21, 2005, to be published.
- [37] D. B. Leeson, "A simple model of feedback oscillator noise spectrum," *Proc. IEEE*, vol. 54, pp. 329-330, Feb. 1966.
- [38] S. Lee and C. T.-C. Nguyen, "Influence of automatic level control on μmechanical resonator oscillator phase noise," *Proceedings*, 2003 IEEE Int. Freq. Control Symp, Tampa, Florida, May 5-8, 2003, pp. 341-349.
- [39] S. Lee and C. T.-C. Nguyen, "Mechanically-coupled micromechanical arrays for improved phase noise," *Proceedings*, IEEE Int. Ultrasonics, Ferroelectrics, and Frequency Control 50th Anniv. Joint Conf., Montreal, Canada, Aug. 24-27, 2004, pp. 280-286.
- [40] Y.-W. Lin, S.-S. Li, Z. Ren, and C. T.-C. Nguyen, "Low phase noise array-composite micromechanical wine-glass disk oscillator," *Technical Digest*, IEEE Int. Electron Devices Mtg., Washington, DC, Dec. 5-7, 2005, to be published.
- [41] C. T.-C. Nguyen and R. T. Howe, "Microresonator frequency control and stabilization using an integrated micro oven," *Digest of Technical Papers*, the 7<sup>th</sup> International Conference on Solid-State Sensors and Actuators (Transducers'93), Yokohama, Japan, pp. 1040-1043, June 7-10, 1993.
- [42] R. Lutwak, J. Deng, W. Riley, M. Varghese, J. Leblanc, G. Tepolt, M. Mescher, K. K. Serkland, K. M. Geib, and G. M. Peake, "The chip-scale atomic clock - low-power physics package," *Proceedings*, Precise Time and Time Interval (PTTI) Systems and Applications Meeting, Washington, DC, Dec. 7-9, 2004.
- [43] L. Liew, S. Knappe, J. Moreland, H. G. Robinson, L. Hollberg and J. Kitching, "Microfabricated alkali atom vapor cells," *Appl. Phys. Lett.* vol. 84, pp. 2694-2696, April 2004.